





Kohn Anomaly with Spin-Orbit Coupling in Monolayer Graphene: A Method to Determine the Rashba Parameter

Arshak L. Vartanian

Email: vardan@ysu.am

ACS APPLIED ELECTRONIC MATERIALS

pubs.acs.org/acsaelm Article

Kohn Anomaly with Spin-Orbit Coupling in Monolayer Graphene: A Method to Determine the Rashba Parameter

Arshak L. Vartanian*



Cite This: ACS Appl. Electron. Mater. 2025, 7, 6348-6355



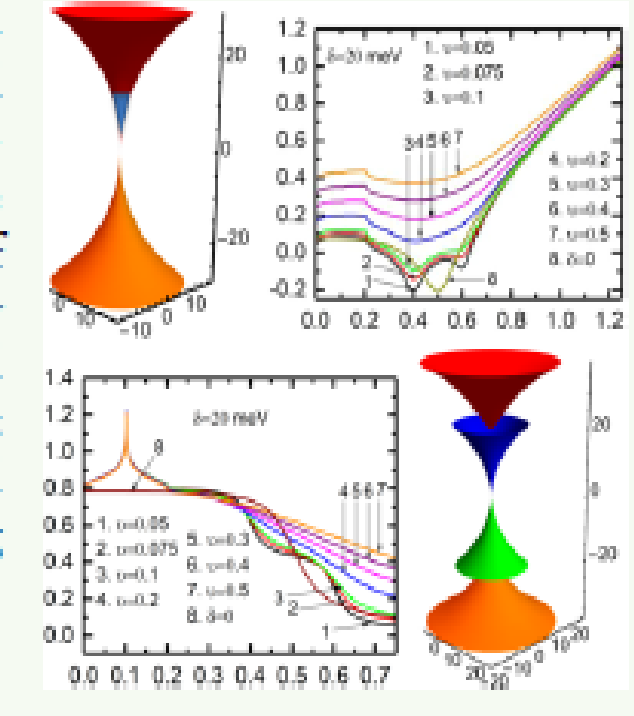
ACCESS

III Metrics & More

Article Recommendations

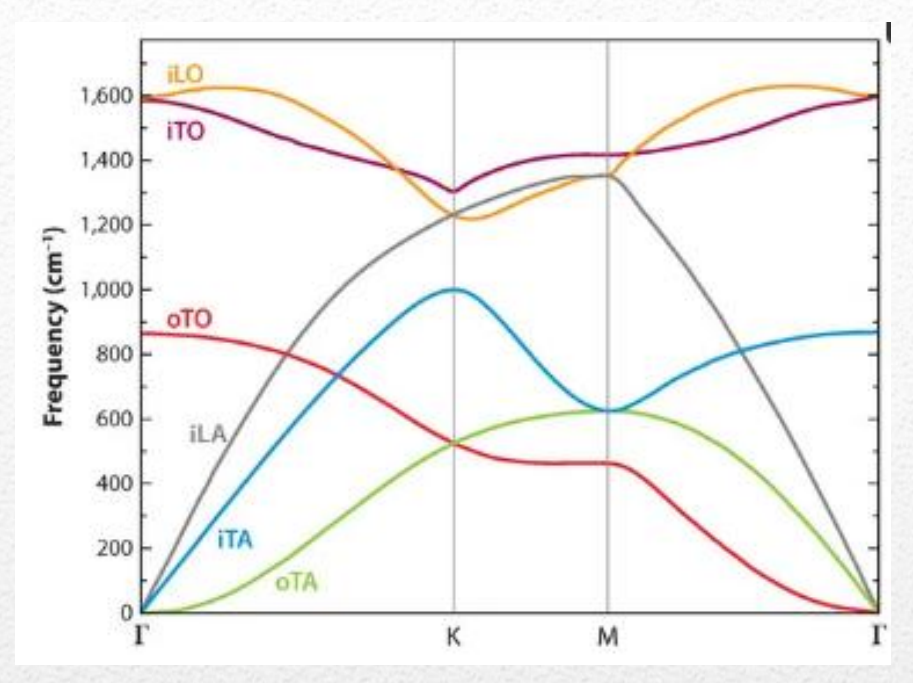
Supporting Information

ABSTRACT: The spin—orbit effect on the quantum corrections to the frequencies of the Γ -point optical phonon modes in graphene within the continuum approximation for phonons and the effective-mass approximation for electrons is first investigated theoretically. The phonon self-energy is calculated in the one-loop approximation, including electron—phonon interaction. The frequency shift and broadening of the optical phonon mode strongly depend on the strength of Rashba spin—orbit coupling (SOC) in graphene. We separately analyze phonon self-energy renormalization due to Rashba SOC and doping in monolayer (ML) graphene. We have obtained the renormalized phonon energy and the broadening of the optical phonon mode by an exact theoretical derivation of the phonon self-energy with Rashba spin—orbit coupling. The obtained results allow the determination of the Rashba SOC parameter values by experimentally studying the mentioned dependencies.

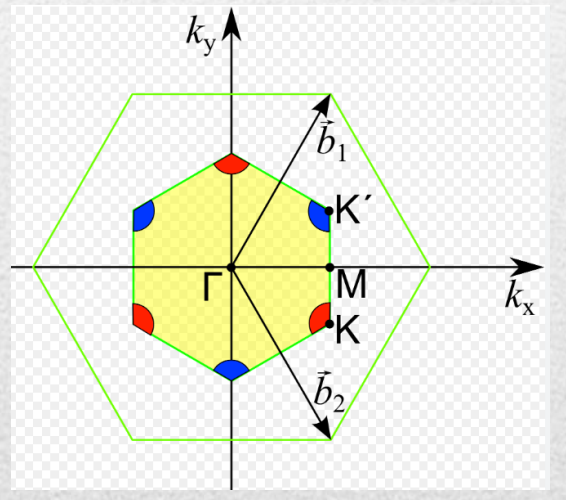


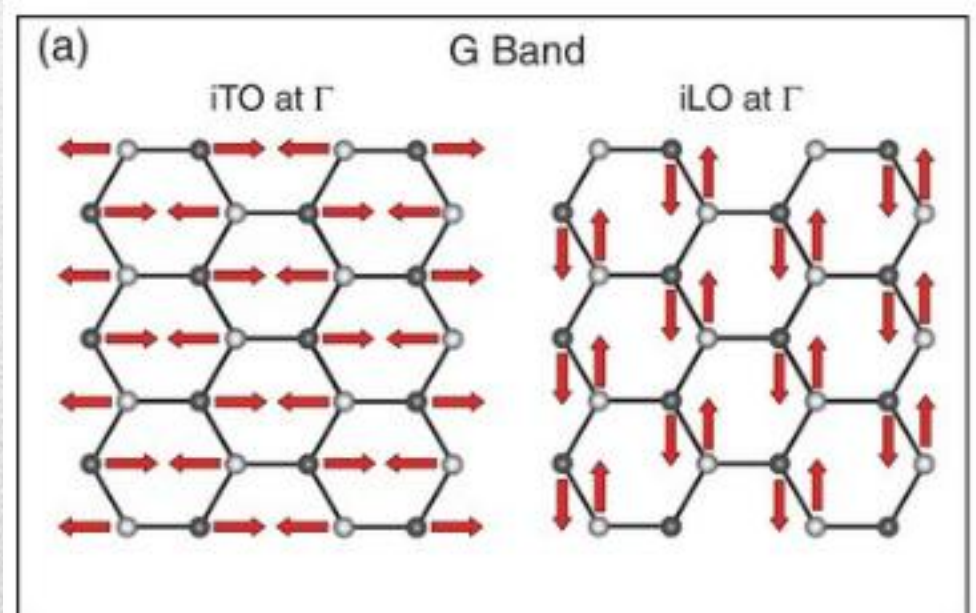
KEYWORDS: graphene, Kohn anomaly, spin-orbit, Rashba parameter, phonon self-energy, experimental method

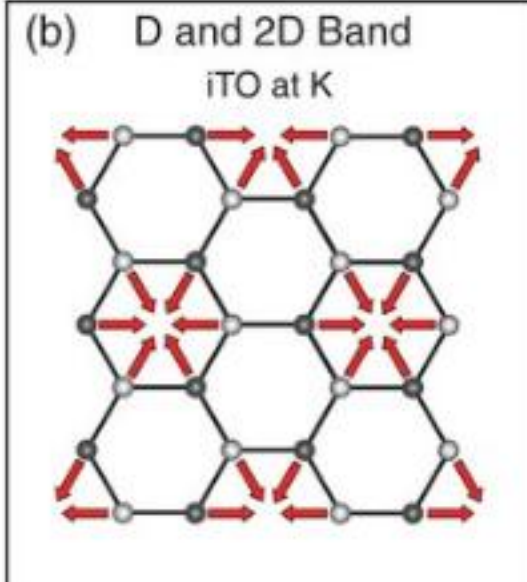
Phonons in Graphene



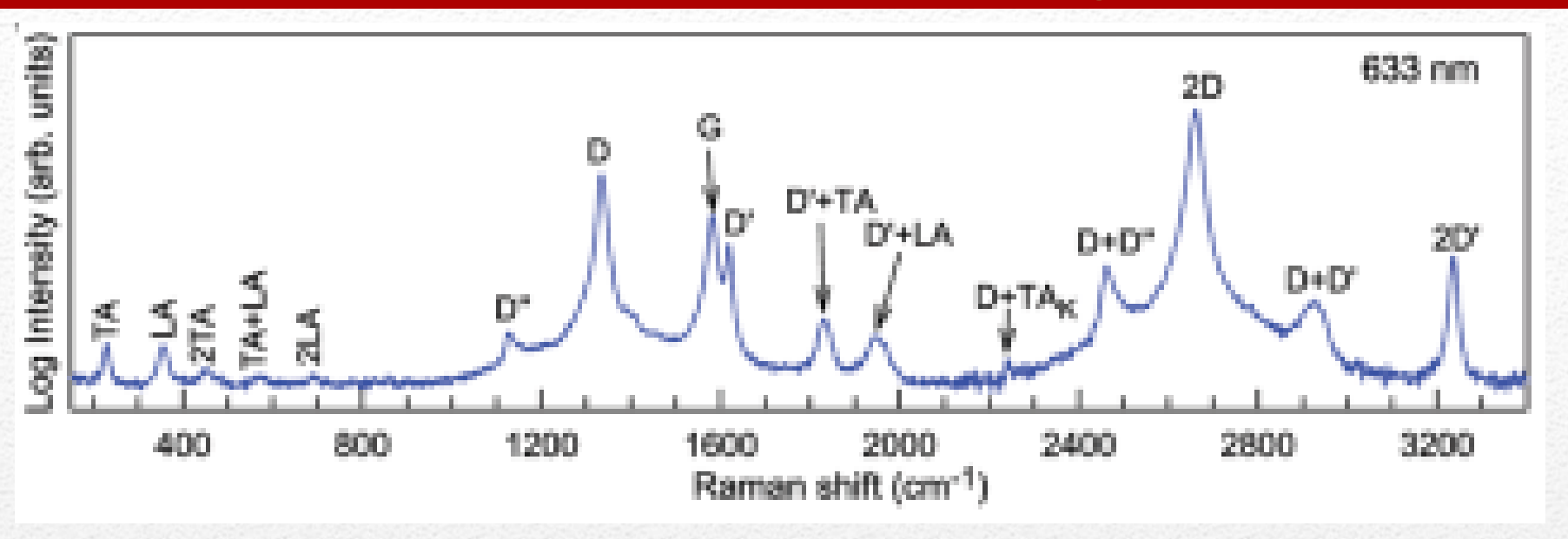
Phonon dispersion of graphene along the high-symmetry lines, Γ-M-K- Γ





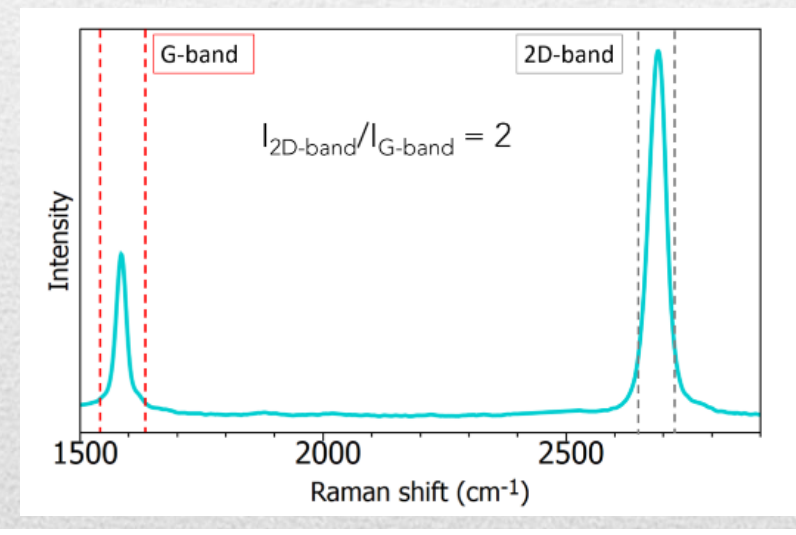


G and **D** bands in Graphene

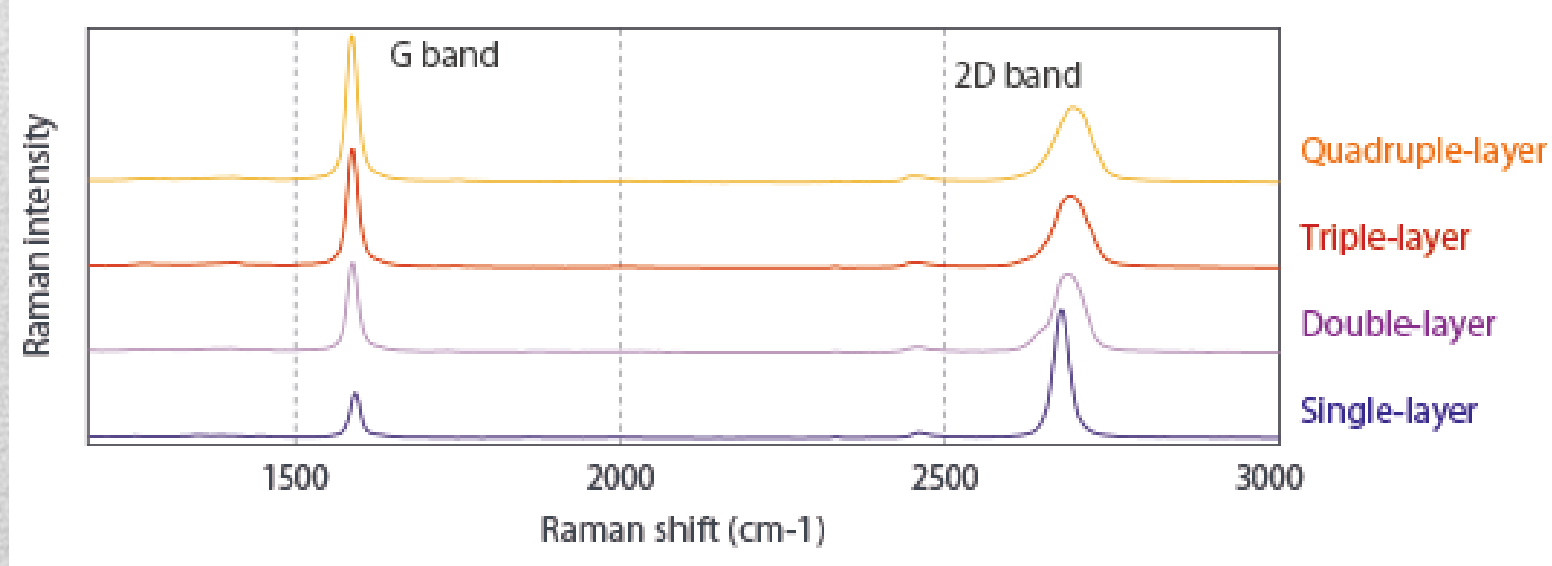


The expected Raman modes observed in graphite whiskers in the spectral region from 150 to 3400 cm⁻¹ excited at 632.8 nm.

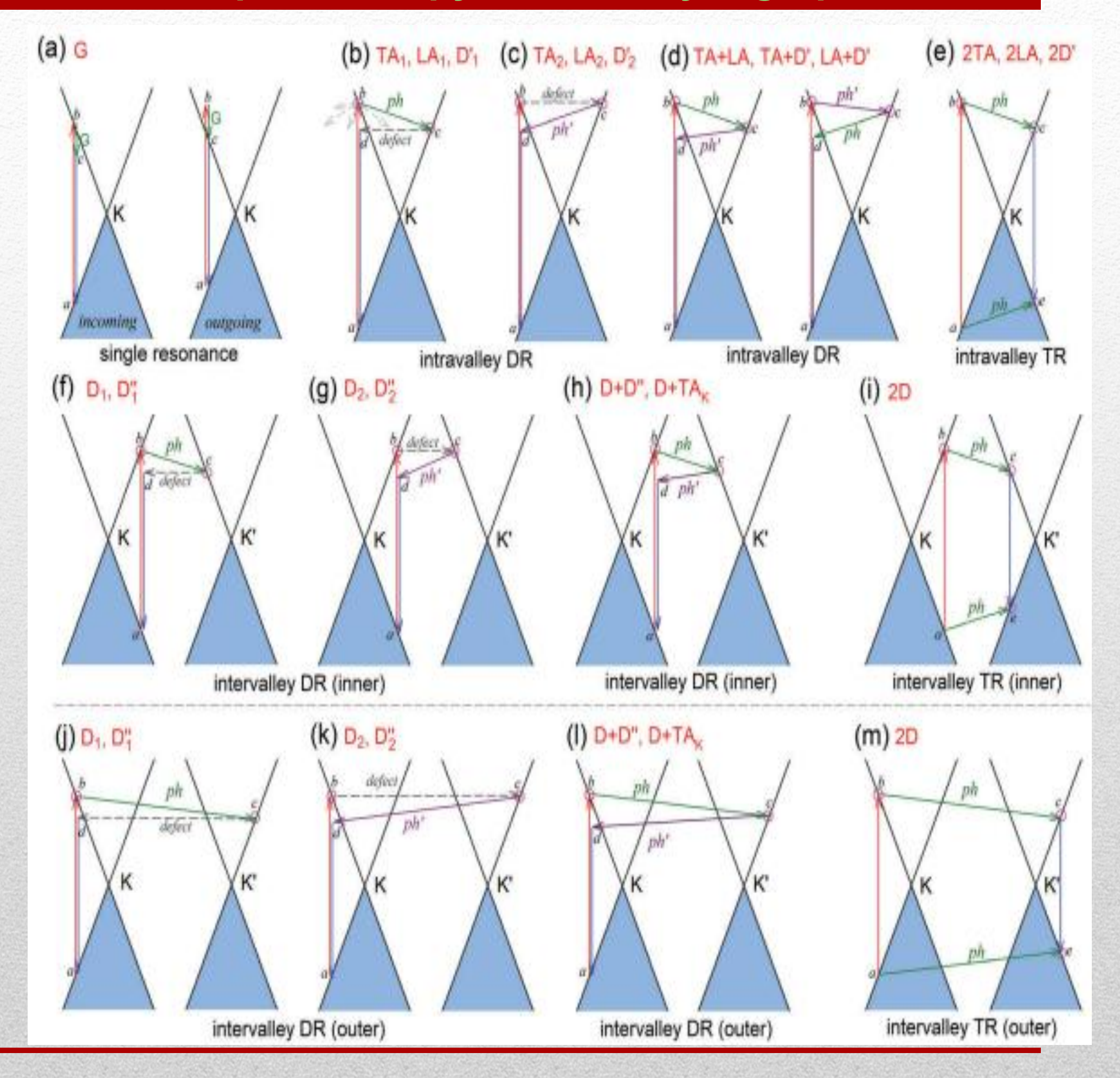
$$\Delta\omega_G = 11(1+n^{1.6})$$



The so-called *D* band locates around 1330–1360 cm⁻¹ and the *G* band near 1580 cm⁻¹.



Raman spectroscopy of monolayer graphene



The Raman resonance processes related to the G, D and 2D points in MG.

The frequency shift and linewidth of the G-band

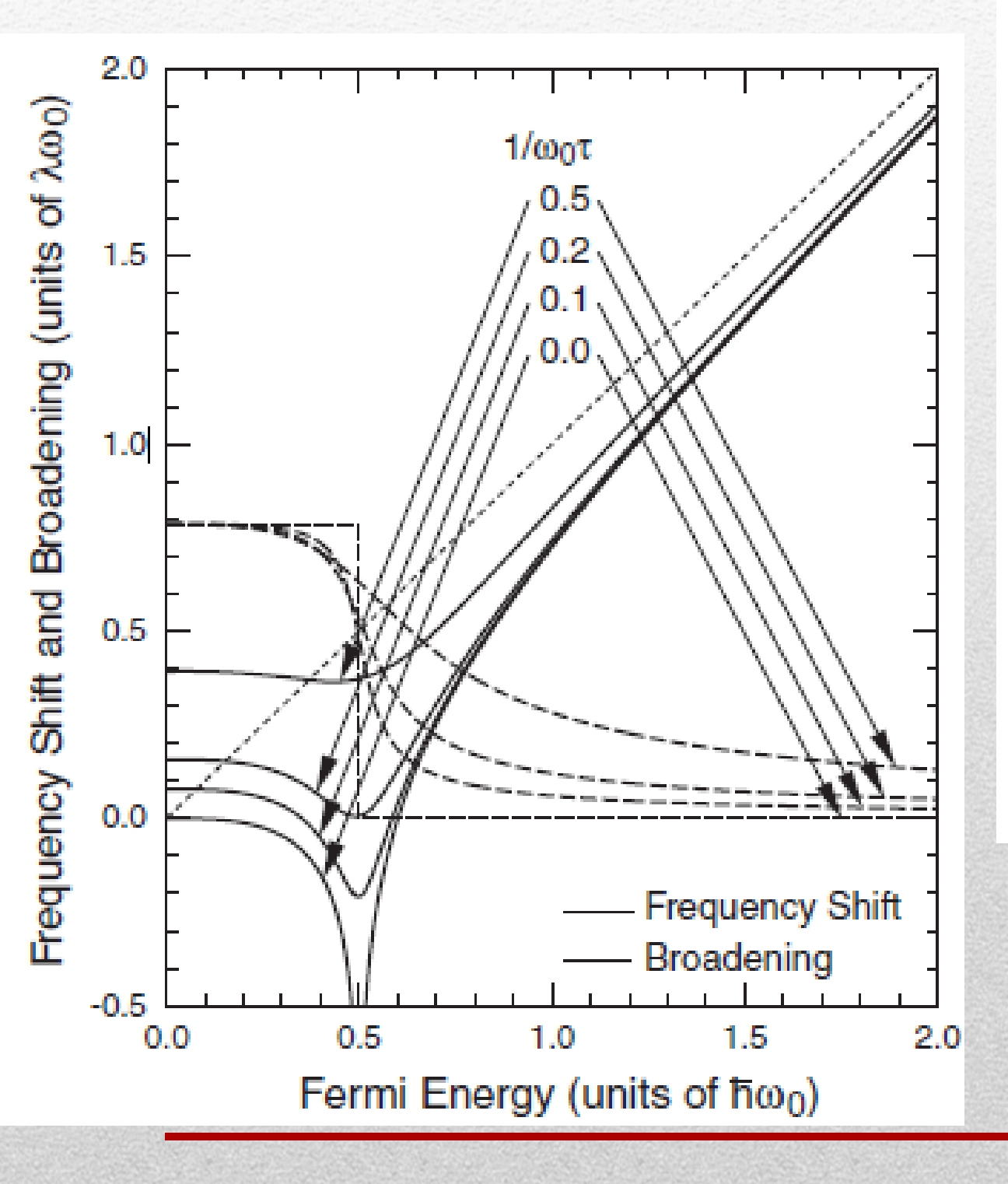
The frequency shift and linewidth of the G-band in graphene were investigated by including:

- Phonon anharmonicity N. Bonini, et al, Phys. Rev. Lett. 99, 176802 (2007)
- Strain effect

 C. Si, Z.Sun,F.Liu, Nanoscale
 8, 3207 (2016)
 - electron-phonon interaction
 T. Ando, J. Phys. Soc. Jpn. 75, 124701 (2006)

Y. Zhao et al., PHYS. REV. B102, 165415 (2020)





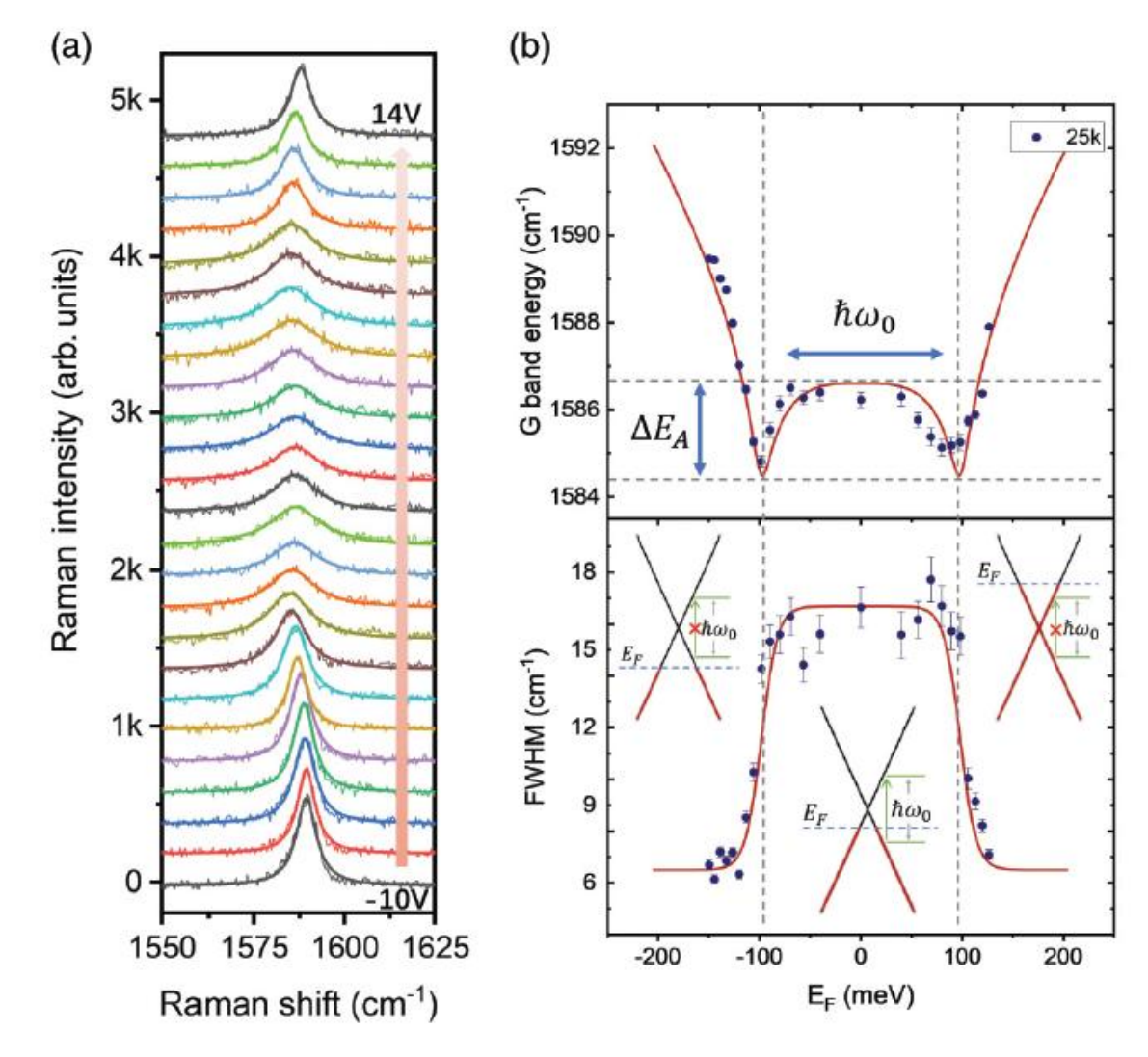


FIG. 2. Fermi energy dependent Raman G mode at 25 K. (a) Raman spectra measured under different back-gate voltages. (b) G band energy (upper panel) and linewidth (lower panel) as a function of Fermi energy. Inset: Landau damping of G phonon into electronhole pairs is only allowed when $|E_{\rm F}| < \frac{\hbar\omega_0}{2}$ and is forbidden by the Pauli principle when $|E_{\rm F}| > \frac{\hbar\omega_0}{2}$. Blue dots: measurements; red lines: theoretical calculation from Eq. (1) with $\zeta = 7.9$ meV.

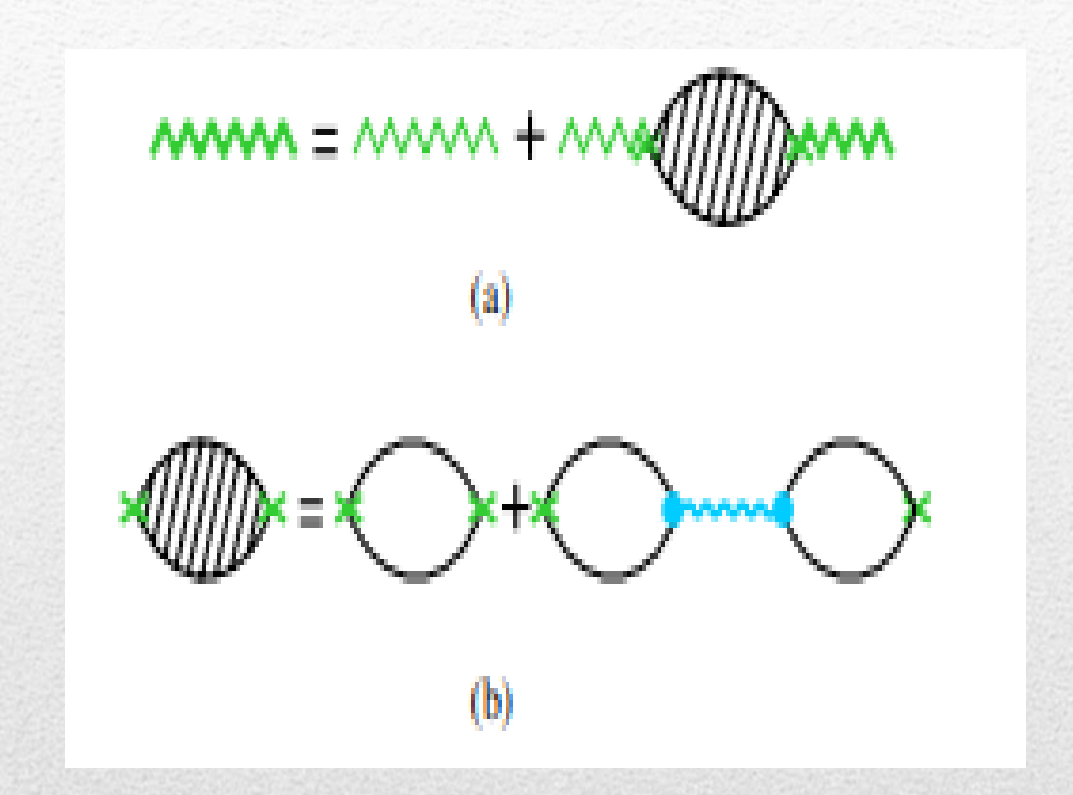


T. Ando, J. Phys. Soc. Japan 75, 124701 (2006)

8

Calculation of the optical phonon self-energy

- (a) The phonon Green function renormalized by direct e-e and e-ph interactions
- (b) Equation for the renormalized phonon self-energy.



$$H = H_0 + \delta(\sigma_x \tau s_y - \sigma_y s_x)$$

$$H_0 = \varepsilon_k (\tau k_x \sigma_x + k_y \sigma_y)$$

 v_F Fermi velocity

$$\varepsilon_k = \hbar v_F k$$
 $\mathbf{k} = (k_x, k_y)$

$$\sigma = (\sigma_x, \sigma_y)
s_s = (s_{sx}, s_{sy})$$
Pauli matrices

$$\begin{cases} \tau = 1, & for K \\ \tau = -1, & for K' \end{cases}$$

$$\varepsilon_{\eta}^{s}(\mathbf{k}) = s\delta + \eta(\delta^{2} + \varepsilon_{k}^{2})^{1/2}$$

$$|\psi_{\eta\tau\mathbf{k}}^{s}\rangle = \left\{2L^{2}\left[1 + \left(\gamma_{\eta\tau\mathbf{k}}^{s}\right)^{2}\right]\right\}^{-1/2} \times e^{i\mathbf{k}\mathbf{r}}\left(-is\tau e^{-i(\tau+1)\theta} - is\tau e^{-i\theta}\gamma_{\eta\tau\mathbf{k}}^{s} e^{-i\tau\theta}\gamma_{\eta\tau\mathbf{k}}^{s} \right)^{T}$$

$$\gamma_{\eta\tau\mathbf{k}}^{s} = \frac{\eta\tau(\delta^{2} + \varepsilon_{k}^{2})^{1/2} + s\delta}{\varepsilon_{k}}$$

$$L^2 \longrightarrow \text{graphene area}$$

$$\begin{cases} \eta = 1, \longrightarrow CB \\ \eta = -1, \longrightarrow VB \end{cases}$$

$$\begin{cases} s = 1, \longrightarrow \uparrow \\ s = -1, \longrightarrow \downarrow \end{cases}$$

$$\Pi(\boldsymbol{q},\omega) = \sum_{\mu} \Pi_{\mu}(\boldsymbol{q},\omega)$$

 μ denotes the optical phonon modes

$$\Pi_{\mu}(\boldsymbol{q},\omega) = -\frac{L^{2}g}{2\pi^{2}} \times \sum_{\boldsymbol{s}\boldsymbol{\eta}\boldsymbol{\tau}} \int_{0}^{\infty} F_{\mu} \binom{s'\boldsymbol{\eta}'\boldsymbol{\tau}'\boldsymbol{k} + \boldsymbol{q}}{s\boldsymbol{\eta}\boldsymbol{\tau}\boldsymbol{k}} \frac{f\left(\varepsilon_{\boldsymbol{\eta}}^{s}(\boldsymbol{k})\right) - f\left(\varepsilon_{\boldsymbol{\eta}'}^{s'}(\boldsymbol{k} + \boldsymbol{q})\right)}{\hbar\omega - \varepsilon_{\boldsymbol{\eta}}^{s}(\boldsymbol{k}) + \varepsilon_{\boldsymbol{\eta}'}^{s'}(\boldsymbol{k} + \boldsymbol{q}) + i0} kdk,$$

$$F_{\mu} \begin{pmatrix} s' \eta' \tau \mathbf{k} \\ s \eta \tau \mathbf{k} \end{pmatrix} = \frac{\left(\gamma_{\eta \tau \mathbf{k}}^{s}\right)^{2} + \left(\gamma_{\eta' \tau \mathbf{k}}^{s'}\right)^{2} + 2ss' \gamma_{\eta \tau \mathbf{k}}^{s} \gamma_{\eta' \tau \mathbf{k}}^{s'}}{\sqrt{\left(1 + \left(\gamma_{\eta \tau \mathbf{k}}^{s}\right)^{2}\right) \left(1 + \left(\gamma_{\eta' \tau \mathbf{k}}^{s'}\right)^{2}\right)}},$$

$$g = \frac{\hbar}{NM\omega_0} \left(\frac{\beta\zeta}{b^2}\right)^2$$

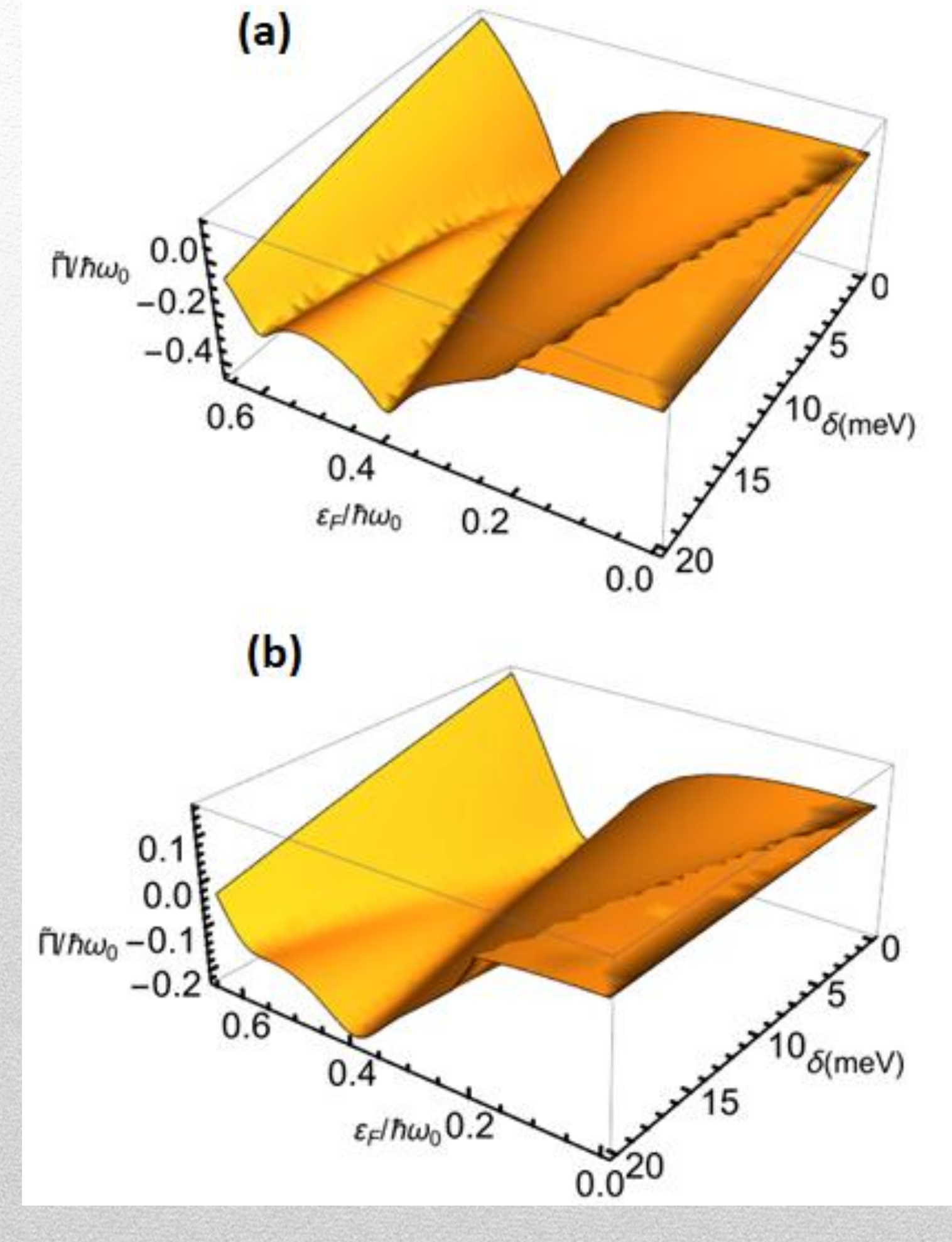
$$\begin{split} \Pi_{\mu}(\omega) &= -\frac{\lambda}{4} \int_{0}^{\infty} \varepsilon d\varepsilon \times \\ &\left\{ \frac{\delta^2}{\varepsilon \sqrt{\varepsilon^2 + \delta^2}} \left[\frac{f\left(\delta + \sqrt{\varepsilon^2 + \delta^2}\right) - f\left(-\delta + \sqrt{\varepsilon^2 + \delta^2}\right)}{\hbar \omega - 2\delta + i0} + \frac{f\left(-\delta + \sqrt{\varepsilon^2 + \delta^2}\right) - f\left(\delta + \sqrt{\varepsilon^2 + \delta^2}\right)}{\hbar \omega + 2\delta + i0} + \frac{f\left(\delta - \sqrt{\varepsilon^2 + \delta^2}\right) - f\left(-\delta - \sqrt{\varepsilon^2 + \delta^2}\right)}{\hbar \omega - 2\delta + i0} + \frac{f\left(-\delta - \sqrt{\varepsilon^2 + \delta^2}\right) - f\left(\delta - \sqrt{\varepsilon^2 + \delta^2}\right)}{\hbar \omega + 2\delta + i0} \right] + \\ \frac{2(\varepsilon^2 + \delta^2)}{\varepsilon \sqrt{\varepsilon^2 + \delta^2}} \left[\frac{f\left(\delta + \sqrt{\varepsilon^2 + \delta^2}\right) - f\left(\delta - \sqrt{\varepsilon^2 + \delta^2}\right)}{\hbar \omega - 2\sqrt{\varepsilon^2 + \delta^2} + i0} + \frac{f\left(-\delta + \sqrt{\varepsilon^2 + \delta^2}\right) - f\left(-\delta - \sqrt{\varepsilon^2 + \delta^2}\right)}{\hbar \omega - 2\sqrt{\varepsilon^2 + \delta^2} + i0} + \frac{f\left(-\delta - \sqrt{\varepsilon^2 + \delta^2}\right) - f\left(-\delta + \sqrt{\varepsilon^2 + \delta^2}\right)}{\hbar \omega + 2\sqrt{\varepsilon^2 + \delta^2} + i0} \right] \right\} \\ \frac{f\left(\delta - \sqrt{\varepsilon^2 + \delta^2}\right) - f\left(\delta + \sqrt{\varepsilon^2 + \delta^2}\right)}{\hbar \omega + 2\sqrt{\varepsilon^2 + \delta^2} + i0} + \frac{f\left(-\delta - \sqrt{\varepsilon^2 + \delta^2}\right) - f\left(-\delta + \sqrt{\varepsilon^2 + \delta^2}\right)}{\hbar \omega + 2\sqrt{\varepsilon^2 + \delta^2} + i0} \right] \right\} \end{split}$$

$$\Delta \omega = (1/\hbar) Re \widetilde{\Pi}(\boldsymbol{q}, \omega), \qquad \Omega = -(1/\hbar) Im \Pi(\boldsymbol{q}, \omega)$$
$$\widetilde{\Pi}(\boldsymbol{q}, \omega) = \Pi(\boldsymbol{q}, \omega) - \Pi(\boldsymbol{q}, 0) \qquad \omega_{L0} = \omega_{T0} = \omega_0$$

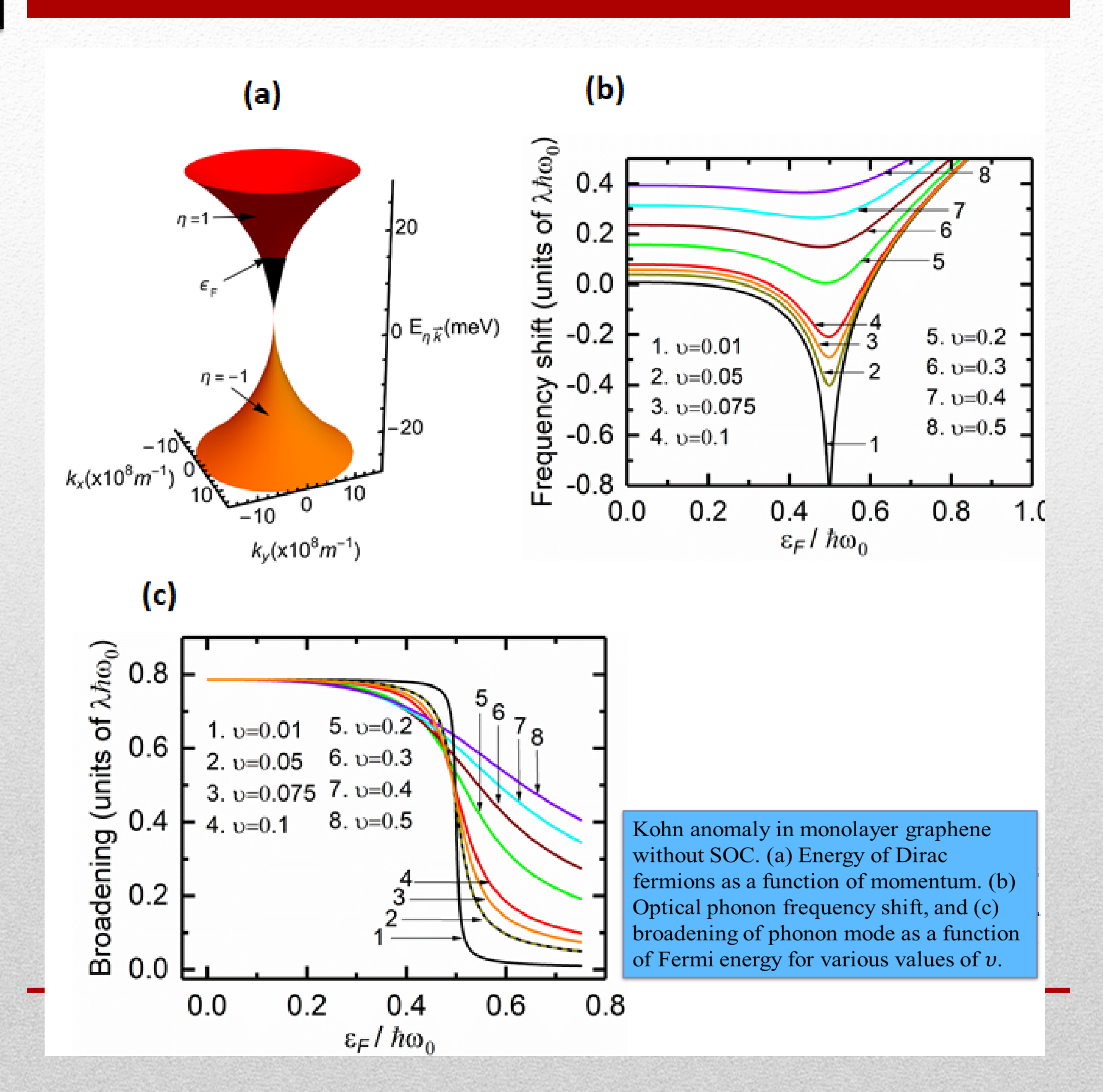
 $\Pi(q,\omega) \longrightarrow$ Phonon total self-energy

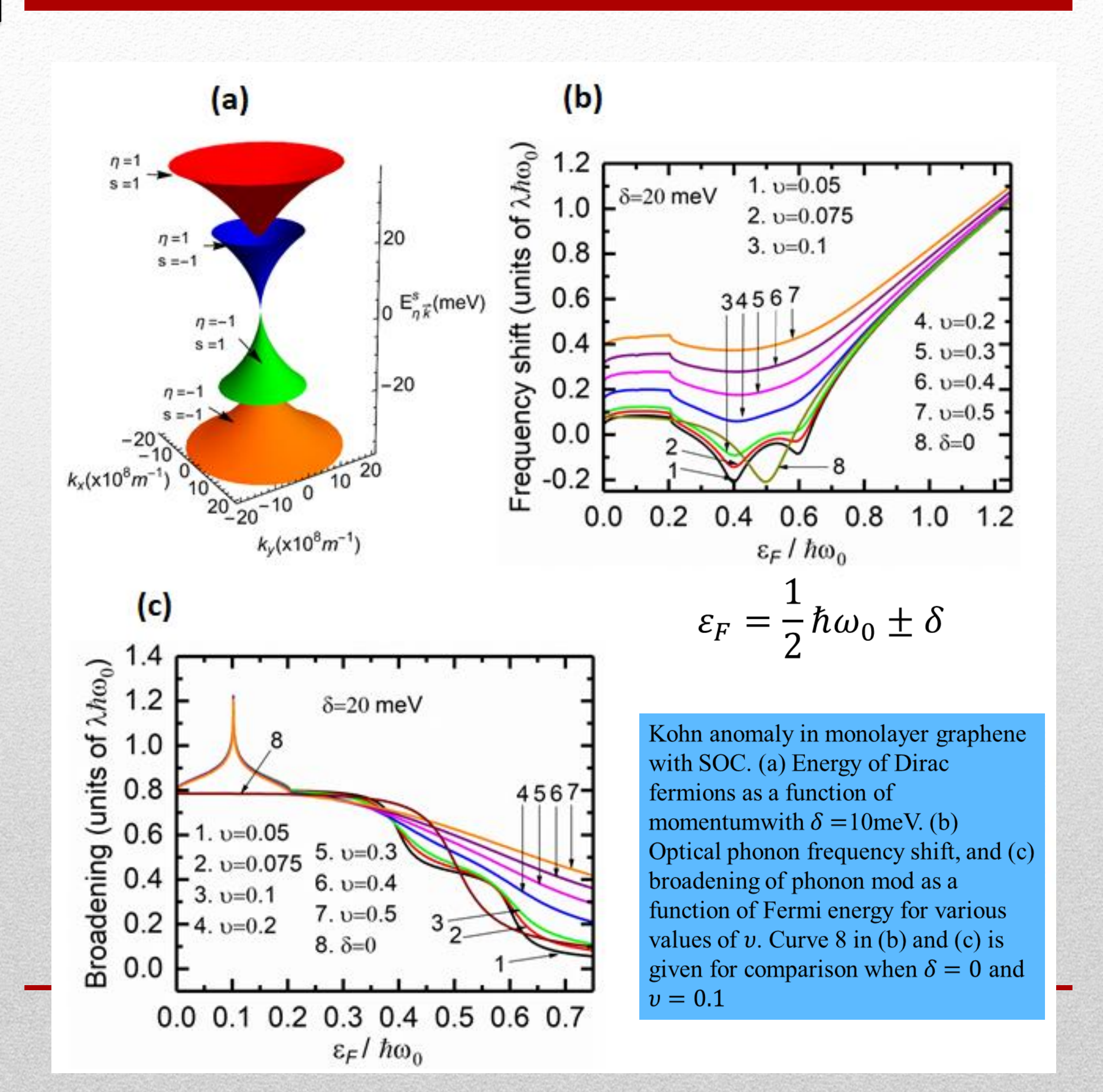
$$\widetilde{\Pi}(w, \varepsilon_F, \delta) = \frac{\lambda w}{4} \left\{ \frac{2w\delta}{w^2 - 4\delta^2} [D_+(0) - D_-(0)] - \frac{iw}{\sqrt{w^2 - 4\delta^2}} [\pi - D_-(w) - D_+(w)] \right\} + \frac{\lambda}{2} \left[\sqrt{\varepsilon_F(\varepsilon_F - 2\delta)} + \sqrt{\varepsilon_F(\varepsilon_F + 2\delta)} - \delta D_-(0) - \delta D_+(0) \right]$$

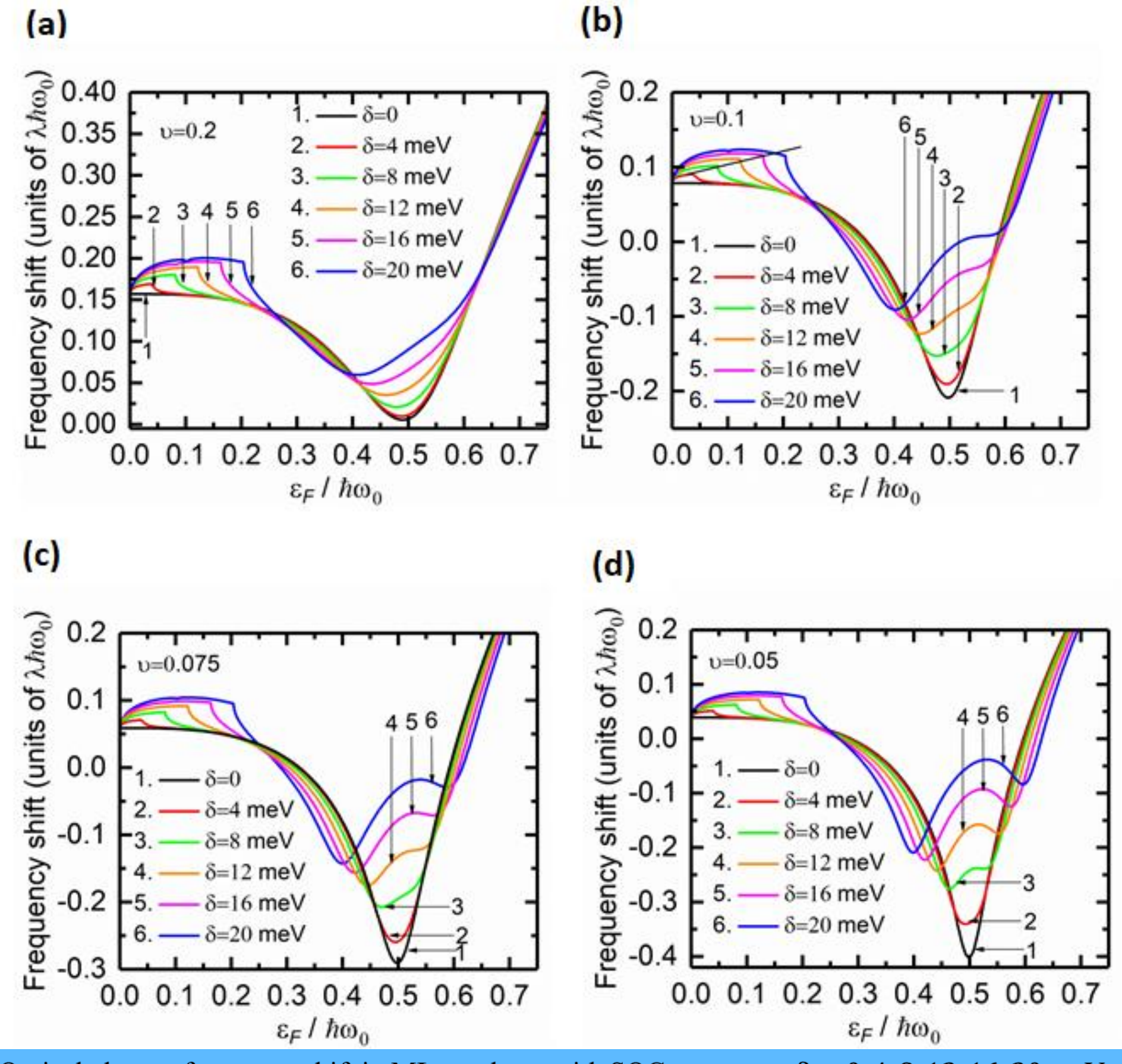
$$D_{\pm}(x) = \arctan\left(i2\sqrt{\varepsilon_F(\varepsilon_F \pm 2\delta)}/\sqrt{x^2 - 4\delta^2}\right)$$
$$w = \hbar\omega + iv\hbar\omega_0$$



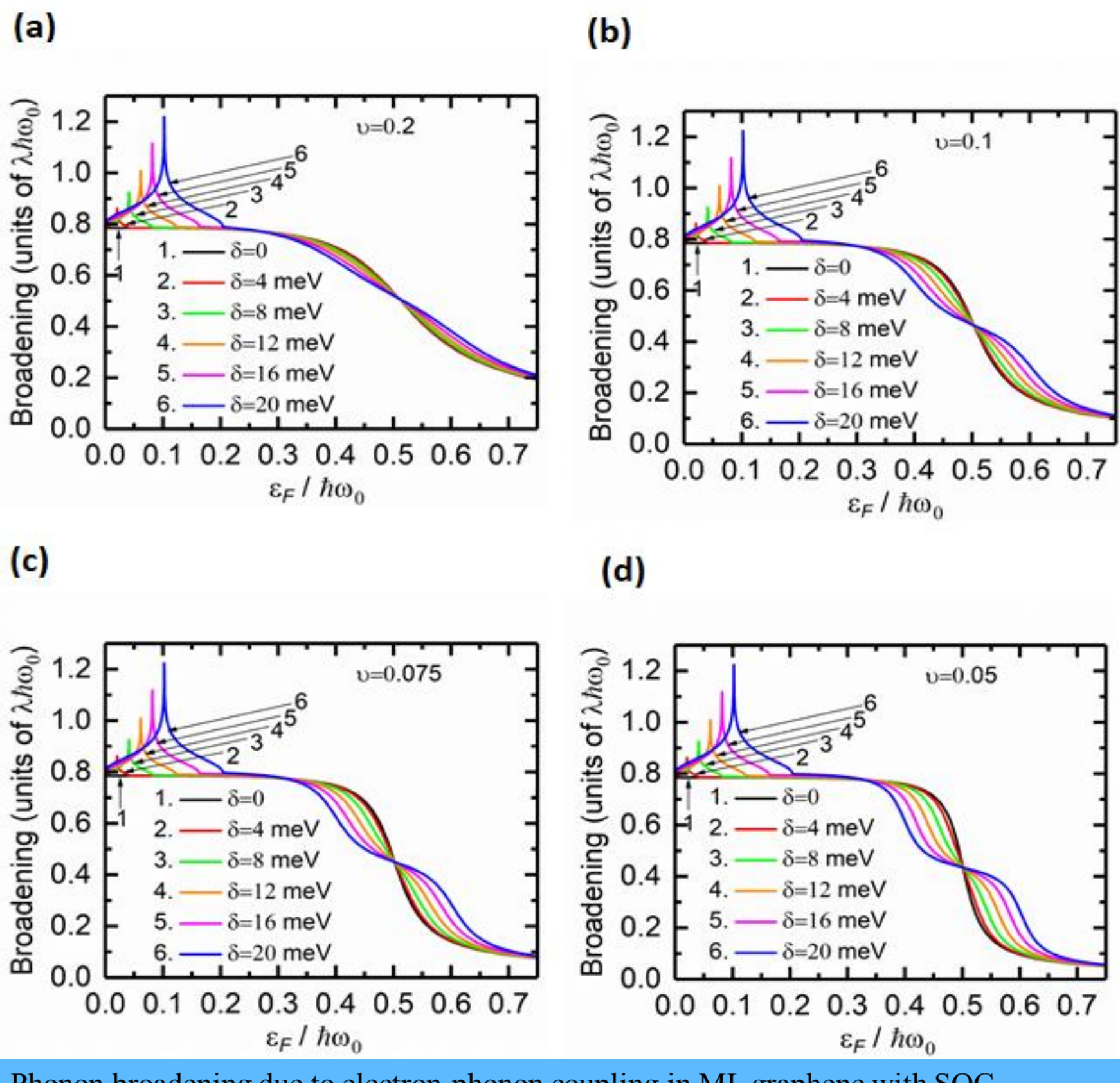
Phonon self-energy $\widetilde{\Pi}(w, \varepsilon_F, \delta)$ versus $\varepsilon_F/\hbar\omega_0$ and δ at (a) v=0.04 and (b) v=0.1.







Optical phonon frequency shift in ML graphene with SOC parameter $\delta = 0, 4, 8, 12, 16, 20$ meV and (a) v = 0.2, (b) v = 0.1, (c) v = 0.075, (d) v = 0.05.



Phonon broadening due to electron-phonon coupling in ML graphene with SOC parameter $\delta = 0, 4, 8, 12, 16, 20$ meV and (a) v = 0.2, (b) v = 0.1, (c) v = 0.075, (d) v = 0.05.

CONCLUSION

By studying the changes in the optical phonon frequency and phonon line broadening at the Gamma point, depending on the Fermi energy, it was shown that in the observation range of the Kohn anomaly:

- a) singularities are observed in the frequency change curve, when the Fermi energy $\varepsilon_F = 2\delta$, where δ is the Rashba parameter,
- b) the Kohn minimum due to the spin-orbit interaction broadens and then turns into two minima at the points $\varepsilon_F/\hbar\omega_0=0.5\pm\delta/\hbar\omega_0$,
- c) a singularity appears at the point $\varepsilon_F = \delta$ in the phonon line broadening curve.

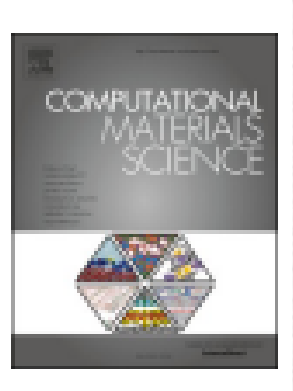
The registration of the mentioned singularities in the experiment provides the determination of the Rashba parameter in the graphene system.



Contents lists available at ScienceDirect

Computational Materials Science





Full Length Article

Exciton-optical phonon coupling in non-spherical quantum dots: A resonant Raman study of InP/ZnSe nanocrystals

A.L. Vartanian a, A.L. Asatryan a, A.H. Movsisyan a, L.A. Vardanyan b, N. Del Fatti c,d, F. Vallée c

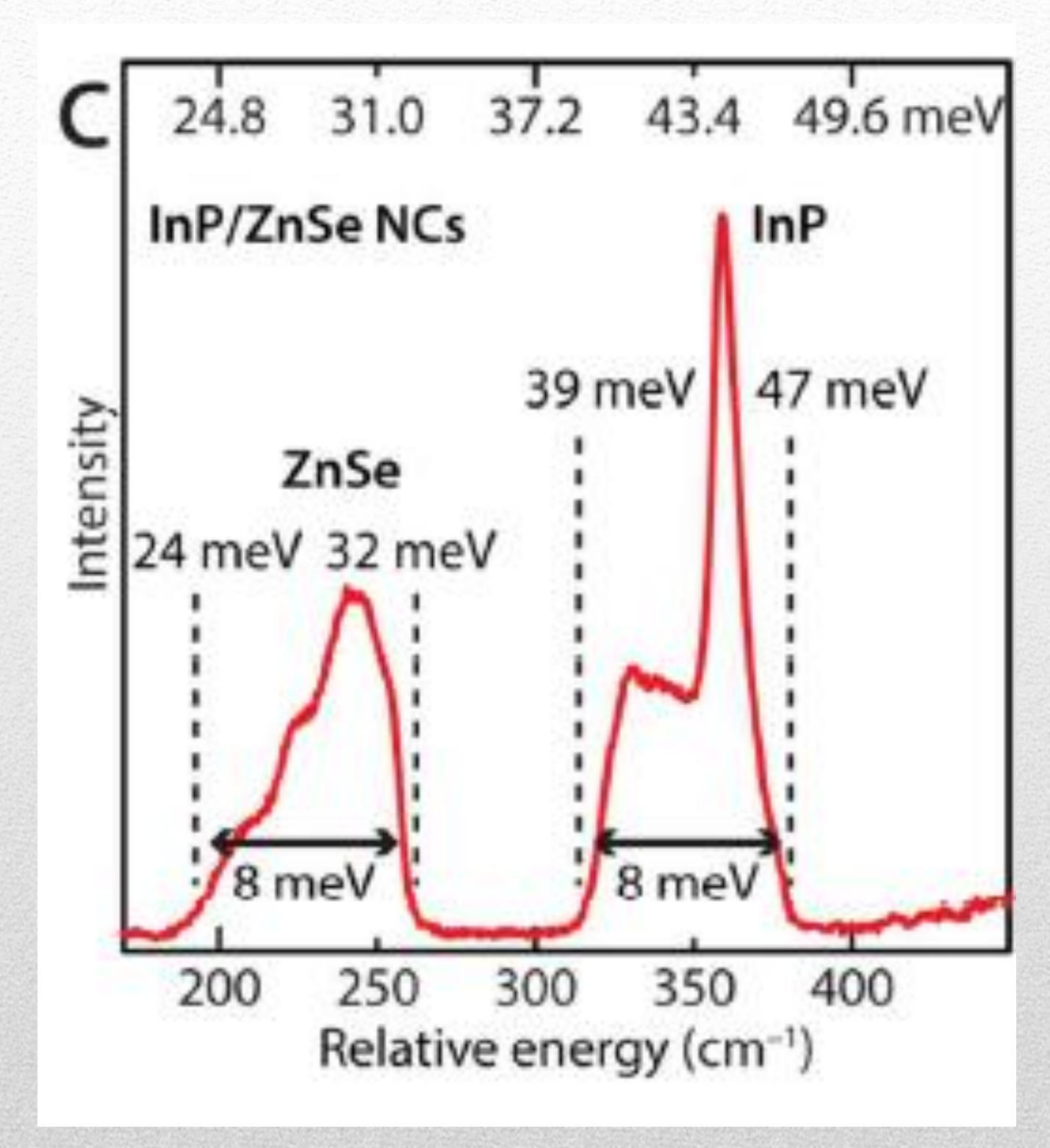
- ^a Department of Solid State Physics, Yerevan State University, 1, Al. Manoogian, Yerevan 0025, Armenia
- b Center of Sciences and Advanced Technologies, Norashen 45-99, Yerevan 0048, Armenia
- ^c Université de Lyon, CNRS, Université Claude Bernard Lyon 1, Institut Lumière Matière, 69622 Villeurbanne Cedex, France
- d Institut Universitaire de France (IUF), 1 rue Descartes, 75231 Paris 05, France

ARTICLE INFO

Keywords: Exciton fine structure Phonon confinement Colloidal quantum dot Resonant Raman scattering InP/ZnSe

ABSTRACT

A theory of first-order resonance Raman scattering by exciton-polar optical phonon (confined and interface) interaction in a core/shell colloidal quantum dot is developed including corrections for non-sphericity. For this purpose both hole energy correction due to the non-sphericity of the quantum dot core and the effect of the electron-hole exchange coupling on the exciton states have been taken into account to calculate the matrix elements of the exciton-phonon Fröhlich interaction. Considering the exciton fine structure, the Raman scattering efficiency and the differential cross- section have subsequently been computed both for confined and interface phonon modes. It is shown that increase of the ellipticity of the dot core strongly alters the resonant Raman spectral profile stressing its key importance in analysis of the experimental data.



Raman peaks related to the ZnSe and InP optical phonons of the InP/ZnSe core/shell QD.

A. Brodu *et al.* Exciton Fine Structure and Lattice Dynamics in InP/ZnSe Core/Shell Quantum Dots. **ACS Photonics 2018, 5, 3353–3362**

The ground-state of the exciton in spherical QD

$$\psi_e^{\sigma_z}(\mathbf{r}_e) = \theta(r_c - r_e) \sqrt{\frac{2\pi^2}{r_c^3}} j_0 \left(\frac{\pi r_e}{r_c}\right) Y_{00}(\vartheta, \varphi) |\sigma_z\rangle, \qquad E_e = \frac{\hbar^2 \pi^2}{2m_e r_c^2}$$

$$\psi_h^M(\mathbf{r}) = 2 \sum_{l=0,2} R_l(r) \sum_{\mu+m=M} {3/2 \choose \mu} \frac{l}{m} \frac{3/2}{-M} Y_{lm}(\vartheta, \varphi) |u_\mu\rangle$$

$$\Phi_F^{ex}(\mathbf{r}_e, \mathbf{r}_h) = \psi_e^{\sigma_z}(\mathbf{r}_e) \psi_h^M(\mathbf{r}_h) \quad \begin{cases} \psi_e^{\sigma_z}(\mathbf{r}_e), & \text{single-electron WF} \\ \psi_h^M(\mathbf{r}_h), & \text{single-hole WF} \end{cases}$$

$$R_l(r) = \theta(r_c - r) \frac{C}{r_c^{3/2}} \left[j_l \left(\frac{kr}{r_c} \right) - (-1)^{l/2} \frac{j_0(k)}{j_0(\sqrt{\beta_h}k)} j_l \left(\frac{\sqrt{\beta_h}kr}{r_c} \right) \right]$$

Designations

$$j_l(x)$$
 Spherical Bessel function

$$M = \pm 3/2, \qquad \pm 1/2$$

 $\mu = \pm 3/2, \qquad \pm 1/2$

$$Y_{lm}(\vartheta,\varphi)$$
 \Longrightarrow Spherical harmonics

$$|u_{\mu}\rangle$$
 Bloch functions of the Γ_8

$$\begin{pmatrix} i & j & k \\ i_1 & j_1 & k_1 \end{pmatrix}$$
 \longrightarrow 3j Wigner symbols

$$E_h = \frac{\hbar^2 k^2}{2m_h r_c^2}$$

$$j_0(k)j_2(\sqrt{\beta_h}k) + j_2(k)j_0(\sqrt{\beta_h}k) = 0$$

$$j_0(k)j_2(\sqrt{\beta_h}k) + j_2(k)j_0(\sqrt{\beta_h}k) = 0$$

$$\widehat{H}_{sh} = \zeta \left\{ \frac{2\widehat{H}_L}{3} - \frac{\hbar^2 k_z^2}{\beta_h m_h} + \left(1 - \frac{1}{\beta_h}\right) \left[\frac{\hbar^2 k_z^2}{8m_h} - \frac{\hbar^2 (k_z J_z) (\hat{\mathbf{k}} \hat{\mathbf{J}})}{2m_h} \right] \right\}$$

$$\widehat{H}_L = \left(\gamma_1 + \frac{5}{2}\gamma\right) \frac{\widehat{\mathbf{p}}^2}{2m_0} - \frac{\gamma}{m_0} \left(\widehat{\mathbf{p}}\widehat{\mathbf{j}}\right)^2$$

$$\widehat{H}_{sh} = \zeta \left\{ \frac{2\widehat{H}_L}{3} - \frac{\hbar^2 k_z^2}{\beta_h m_h} + \left(1 - \frac{1}{\beta_h}\right) \left[\frac{\hbar^2 k_z^2}{8m_h} - \frac{\hbar^2 (k_z J_z) (\hat{\mathbf{k}} \hat{\mathbf{J}})}{2m_h} \right] \right\}$$

$$r_c = (a^2c)^{1/3}$$
 $\zeta = 3(c/r_c - 1)/2$ $\Delta = \zeta E_h u(\beta_h)$ $\widehat{H}_{exch} = -\eta(\sigma \mathbf{J})$

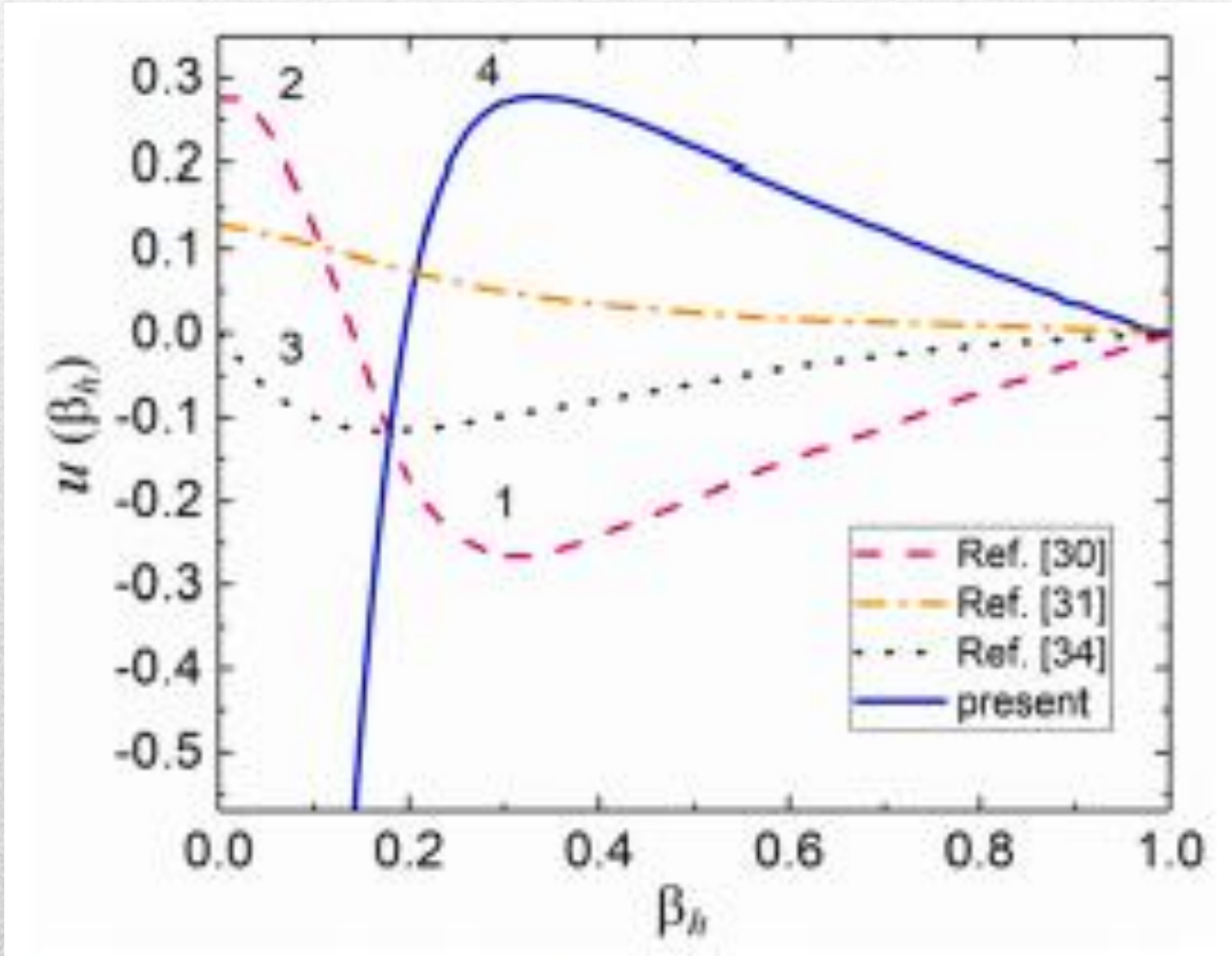


Fig. 1. The dimensionless function $u(\beta_h)$ associated with hole ground state energy splitting for different confining potentials.

$$\tau_{\nu} = \left\{ 1/2 + (-1)^{\nu+1} (-\eta + \Delta/2)/2 [(-\eta + \Delta/2)^2 + 3\eta^2]^{1/2} \right\}^{1/2}$$

	Exciton wave functions	Exciton energies
Φ_{-2}^{ex}	$\psi_e^{\downarrow}(\mathbf{r}_e)\psi_h^{-3/2}(\mathbf{r}_h)$	$E_0 - 3\eta/2 - \Delta/2$
Φ_2^{ex}	$\psi_e^{\uparrow}(\mathbf{r}_e)\psi_h^{3/2}(\mathbf{r}_h)$	$E_0 - 3\eta/2 - \Delta/2$
Φ_0^{exU}	$2^{-1/2} \left[\psi_e^{\uparrow}(\mathbf{r}_e) \psi_h^{-1/2}(\mathbf{r}_h) - \psi_e^{\downarrow}(\mathbf{r}_e) \psi_h^{1/2}(\mathbf{r}_h) \right]$	$E_0 + \eta/2 + \Delta/2 + 2\eta$
Φ_0^{exL}	$2^{-1/2} \left[\psi_e^{\uparrow}(\mathbf{r}_e) \psi_h^{-1/2}(\mathbf{r}_h) + \psi_e^{\downarrow}(\mathbf{r}_e) \psi_h^{1/2}(\mathbf{r}_h) \right]$	$E_0 + \eta/2 + \Delta/2 - 2\eta$
Φ_1^{exU}	$ au_1\psi_e^{\uparrow}(\mathbf{r}_e)\psi_h^{1/2}(\mathbf{r}_h)- au_2\psi_e^{\downarrow}(\mathbf{r}_e)\psi_h^{3/2}(\mathbf{r}_h)$	$E_0 + \eta/2 + \sqrt{(-\eta + \Delta/2)^2 + 3\eta^2}$
Φ_1^{exL}	$ au_2\psi_e^{\uparrow}(\mathbf{r}_e)\psi_h^{1/2}(\mathbf{r}_h) + au_1\psi_e^{\downarrow}(\mathbf{r}_e)\psi_h^{3/2}(\mathbf{r}_h)$	$E_0 + \eta/2 - \sqrt{(-\eta + \Delta/2)^2 + 3\eta^2}$
Φ_{-1}^{exU}	$ au_2\psi_e^{\uparrow}(\mathbf{r}_e)\psi_h^{-3/2}(\mathbf{r}_h) - au_1\psi_e^{\downarrow}(\mathbf{r}_e)\psi_h^{-1/2}(\mathbf{r}_h)$	$E_0 + \eta/2 + \sqrt{(-\eta + \Delta/2)^2 + 3\eta^2}$
Φ_{-1}^{exL}	$ au_1\psi_e^{\uparrow}(\mathbf{r}_e)\psi_h^{-3/2}(\mathbf{r}_h) + au_2\psi_e^{\downarrow}(\mathbf{r}_e)\psi_h^{-1/2}(\mathbf{r}_h)$	$E_0 + \eta/2 - \sqrt{(-\eta + \Delta/2)^2 + 3\eta^2}$

$$E_0 = E_g + E_e + E_h$$
, $E_g \Longrightarrow$ Band gap energy
$$H_{ex-ph}^{t,\lambda} = e \Big[\Gamma_{\lambda}^t(\mathbf{r}_h) - \Gamma_{\lambda}^t(\mathbf{r}_e) \Big] a_{\lambda}^t + h.c.$$

$$g_1 = \delta_{j,0} \frac{1}{2\sqrt{\pi}} \int_0^{r_c} \Gamma_{\lambda}^t(r) [R_0^2(r) + R_2^2(r)] r^2 dr$$

$$g_2 = \delta_{j,2} \frac{1}{\sqrt{5\pi}} \int_0^{r_c} \Gamma_{\lambda}^t(r) (R_0(r)R_2(r)) r^2 dr$$

TABLE II. Hole-phonon matrix elements calculated considering the joint influence of the electron-hole exchange interaction and core shape non-sphericity.

	$\langle \Phi^{ex}_{-2} $	$\langle \Phi_2^{ex} $	$\langle \Phi_0^{exU} $	$\langle \Phi_0^{ext} $	$\langle \Phi_1^{exU} $	$\langle \Phi_1^{ext} $	$\langle \Phi_{-1}^{exU} $	$\langle \Phi^{ext}_{-1} $
$ \Phi_{-2}^{ex}\rangle$	$g_1 + g_2$	0	0	$2g_2$	$\sqrt{2}\tau_1g_2$	$\sqrt{2} au_2g_2$	$ \tau_2 g_1 \\ - (\sqrt{2}\tau_1 \\ - \tau_2) g_2 $	$\tau_1 g_1 + (\tau_1 + \sqrt{2}\tau_2)g_2$
$ \Phi_2^{ex}\rangle$	0	$g_1 + g_2$	0	$2g_2$	$- au_{2}g_{1} + (\sqrt{2} au_{1} - au_{2})g_{2}$	1 1 2 2 2 3 9 2	$-\sqrt{2}\tau_1g_2$	
Φ ^{exU} ⟩	$-2g_2$	$2g_2$	g_1-g_2	0	$\begin{array}{c} \frac{1}{\sqrt{2}}\tau_{1}(g_{2}\\ -g_{1})\\ -2\tau_{2}g_{2} \end{array}$	$\begin{array}{c} \frac{1}{\sqrt{2}}\tau_{2}(g_{2}\\ -g_{1})\\ +2\tau_{1}g_{2} \end{array}$	$-g_1$)	$\begin{array}{c} \frac{1}{\sqrt{2}}\tau_{2}(g_{1}\\ -g_{2})\\ -2\tau_{1}g_{2} \end{array}$
$ \Phi_0^{ext} angle$		0	0	$g_1 - g_2$	$-a_{2}$)	- u+1	- u+,	— (4+)
$ \Phi_1^{exU}\rangle$	$\sqrt{2}\tau_1g_2$	$- au_{2}g_{1} - (\sqrt{2} au_{1} + au_{2})g_{2}$	$\frac{1}{\sqrt{2}}\tau_1(g_2$ $-g_1)$	$\frac{1}{\sqrt{2}}\tau_1(g_1 - g_2) - 2\tau_2 g_2$	$g_1 + (au_2^2 - au_1^2) g_2$	$-(\sqrt{2} + 2\tau_1\tau_2)g_2$	$2\sqrt{2}\tau_1\tau_2g_2$	$\sqrt{2}(\tau_1^2 - \tau_2^2)g_2$
$ \Phi_1^{ext} angle$	$\sqrt{2} au_2g_2$	$\tau_1 g_1 + (\tau_1$ $-\sqrt{2}\tau_2)g_2$	$\begin{array}{c} \frac{1}{\sqrt{2}}\tau_2(g_2\\ -g_1) \end{array}$	$rac{1}{\sqrt{2}} au_2(g_2 - g_1) + 2 au_1 g_2$	$(\sqrt{2} - 2\tau_1\tau_2)g_2$	$g_1 - (\tau_2^2 - \tau_1^2)g_2$	$\sqrt{2}(\tau_2^2 - \tau_1^2)g_2$	$2\sqrt{2}\tau_1\tau_2g_2$
$ \Phi_{-1}^{exU}\rangle$	$egin{array}{l} & au_2 g_1 \\ & + (\sqrt{2} au_1 \\ & + au_2) g_2 \end{array}$	$-\sqrt{2}\tau_1g_2$	$\begin{array}{c} \frac{1}{\sqrt{2}}\tau_1(g_2\\ -g_1) \end{array}$	$+ 2\tau_2 g_2$	$2\sqrt{2}\tau_1\tau_2g_2$		$g_1 + (\tau_2^2 - \tau_1^2)g_2$	$(\sqrt{2} + 2\tau_1\tau_2)g_2$
$ \Phi^{ext}_{-1} angle$	$\tau_1 g_1 + (\tau_1 - \sqrt{2}\tau_2)g_2$	$\sqrt{2}\tau_2g_2$	$\frac{1}{\sqrt{2}}\tau_2(g_1\\-g_2)$	$\frac{1}{\sqrt{2}}\tau_2(g_1 - g_2) + 2\tau_1g_2$	$\sqrt{2}(\tau_1^2 - \tau_2^2)g_2$	$2\sqrt{2}\tau_1\tau_2g_2$	$-(\sqrt{2} \\ -2\tau_1\tau_2)g_2$	g_1 $-(\tau_2^2$ $-\tau_1^2)g_2$

$$M(\hbar\Omega_{i},\hbar\Omega_{s};\mathbf{e}_{i},\mathbf{e}_{s},t,\lambda)$$

$$=\sum_{F'F}\frac{\langle 0|H_{rad}|F'\rangle\langle F',N\pm1|H_{ex-ph}^{t,\lambda}|F,N\rangle\langle F|H_{rad}|0\rangle}{(\hbar\Omega_{i}-E_{ex,F}-i\Gamma_{F}/2)(\hbar\Omega_{i}-E_{ex,F'}\mp\hbar\omega_{\lambda}^{t}-i(\Gamma_{F'}+\Gamma_{ph})/2)}$$

 \mathbf{e}_i and Ω_i (\mathbf{e}_s and $\Omega_s = \Omega_i \mp \omega_\lambda^t$



Polarization vector and frequency of the incident (scattered) photon, respectively

differential Raman cross-section

$$\langle \sigma' M', N \pm 1 | H_{ex-ph}^{t,\lambda} | \sigma M, N \rangle$$



Matrix element of exciton-phonon interaction

$$\frac{d^2\rho}{d\Omega_s do} = \frac{V^2 \Omega_s^3 \varkappa(\Omega_i) \varkappa^3(\Omega_s)}{4\pi^2 \hbar c^4 \Omega_i} \sum_{t,\lambda} |M(\hbar\Omega_i, \hbar\Omega_s; \mathbf{e}_i, \mathbf{e}_s, t, \lambda)|^2 \delta(\hbar\Omega_i - \hbar\Omega_s \mp \hbar\omega_\lambda^t)$$

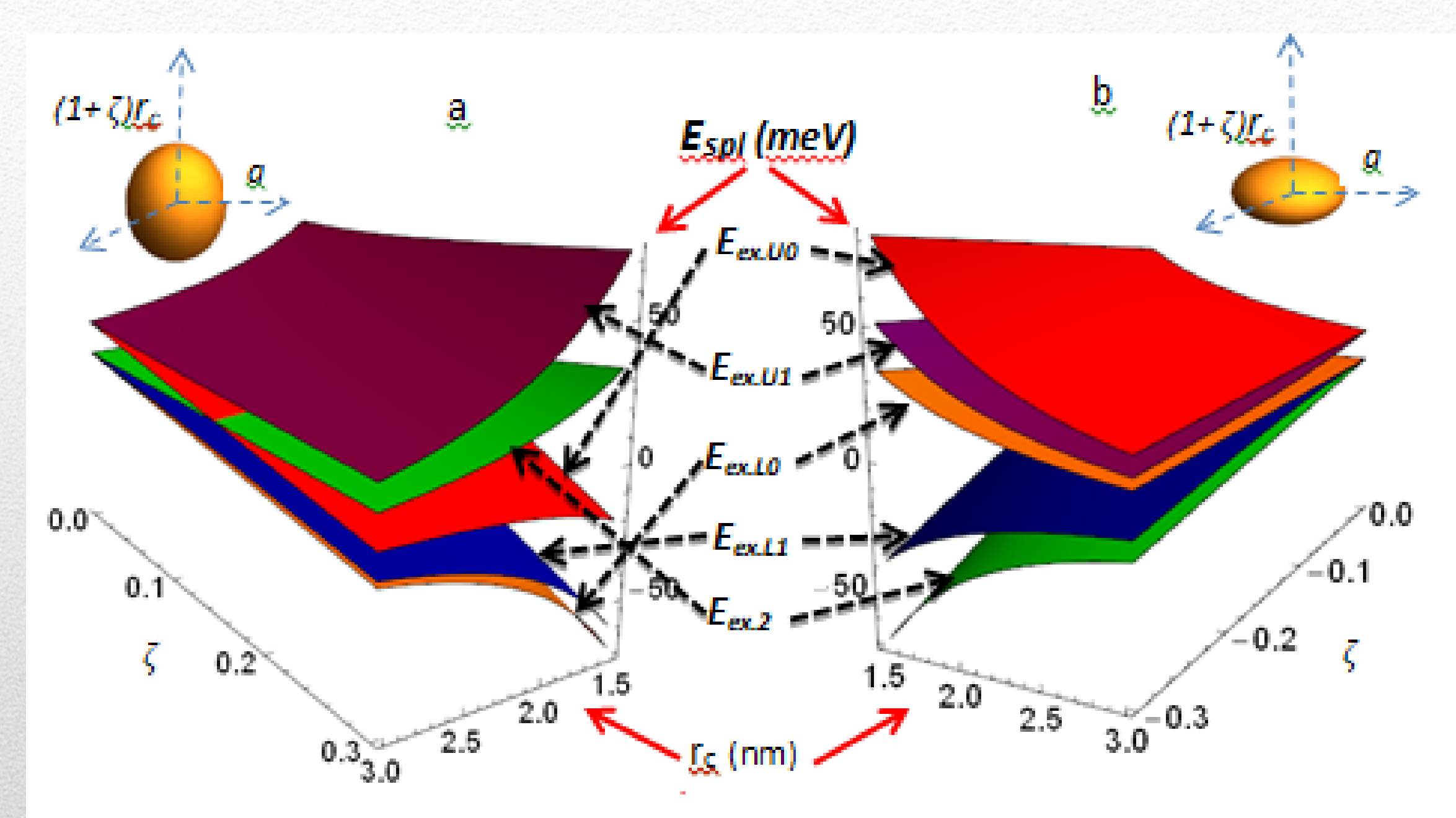


Fig. 2. Exciton fine-structure splitting energies as functions of the core average radius r_c and ellipticity parameter ζ of a core/shell InP/ZnSe CQD for (a) prolate ($\zeta > 0$) and (b) oblate ($\zeta < 0$) core quantum dot. Exciton fine-structure energies are labeled according to exciton total angular momentum projection F (see Table I).

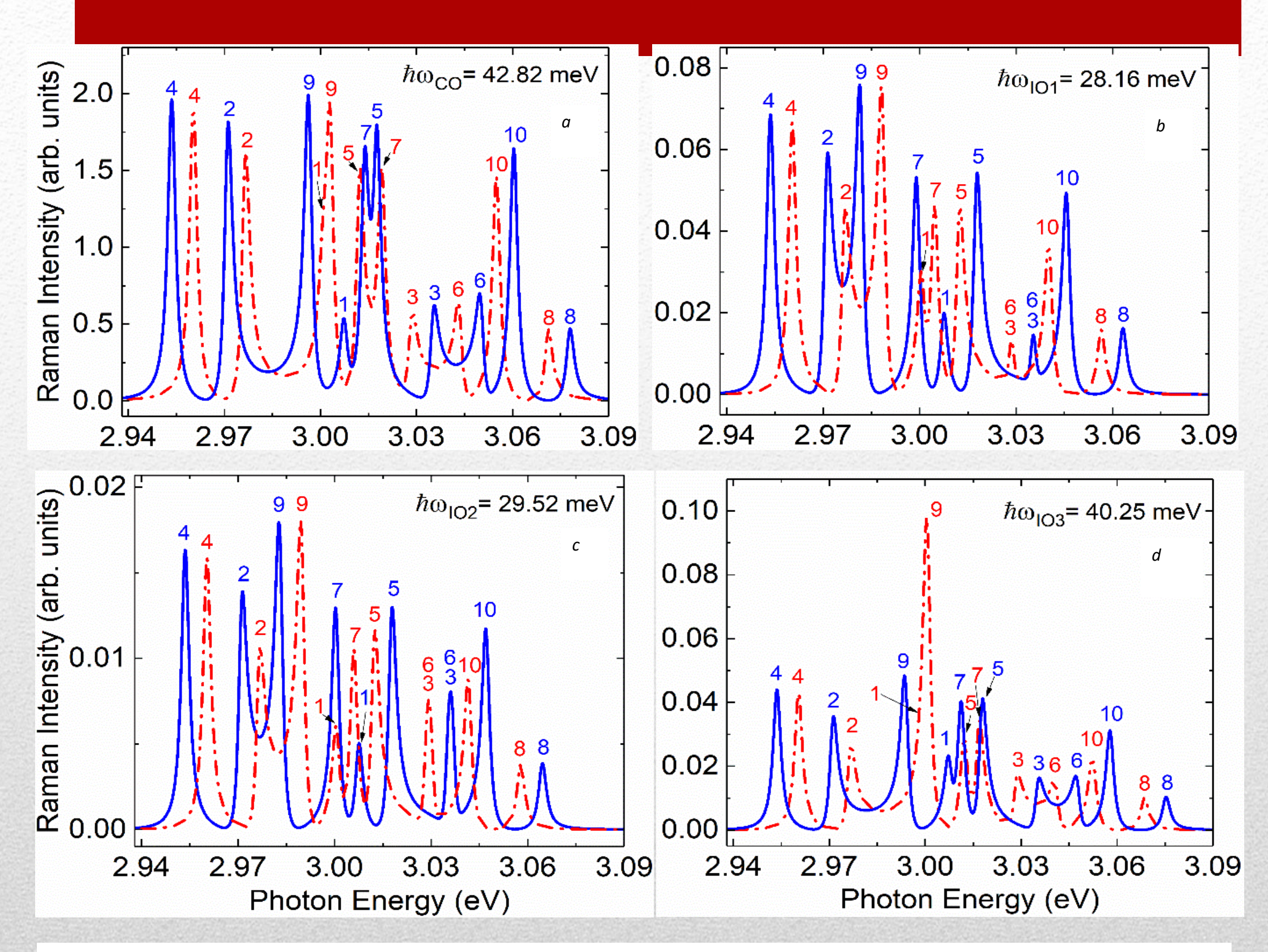


Fig. 4. Computed dependence of the integrated Raman intensity on the photon energy for phonon modes a) CO, b) IO1, c) IO2, d) IO3 in a core/shell InP/ZnSe CQD with oblate core with mean radius $r_c = 2$ nm ($r_s = 2.9$ nm), at 4K and $\Gamma_{\sigma M} = 3$ meV. The peaks labeled 4, 2, 5 and 9, 7, 10 correspond to the incoming and outgoing resonances, respectively, with the Ex_0^U , Ex_1^L , Ex_1^U bright exciton levels. Solid (blue) curves refer to an oblate core with $\zeta = -0.28$ and dashed-dotted (red) curves with $\zeta = -0.21$.

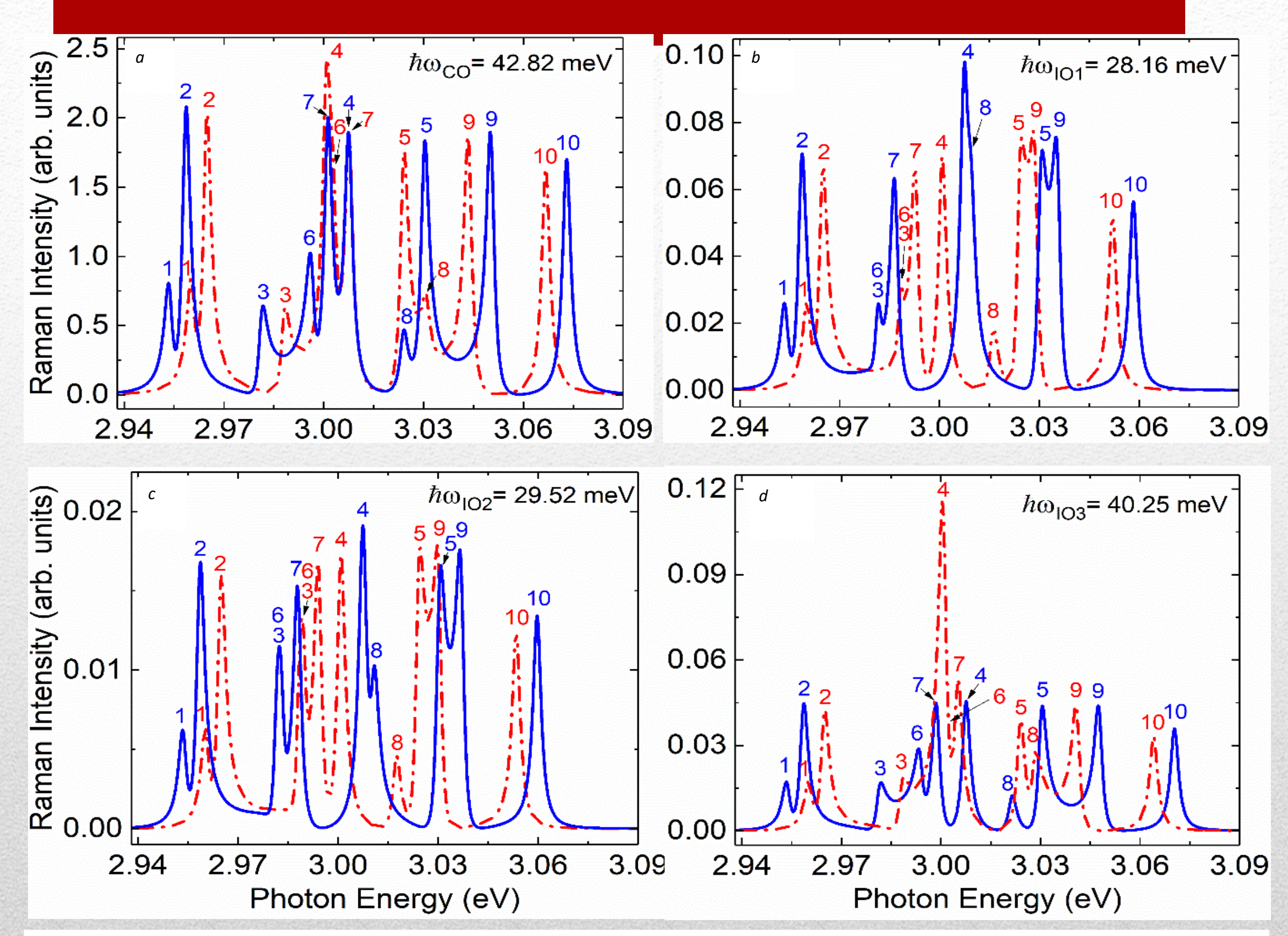


Fig. 3. Computed dependence of the integrated Raman intensity on the photon energy for phonon modes a) CO, b) IO1, c) IO2, d) IO3 in a core/shell InP/ZnSe CQD with prolate core with mean radius $r_c = 2$ nm ($r_s = 2.9$ nm) at 4K and $\Gamma_{\sigma M} = 3$ meV. The peaks labeled 2, 4, 5 and 7, 9, 10 correspond to the incoming and outgoing resonances, respectively, with the Ex_1^L , Ex_0^U , Ex_1^U bright exciton levels. Solid (blue) curves refer to a prolate core with $\zeta = 0.28$ and dashed-dotted (red) curves with $\zeta = 0.21$.

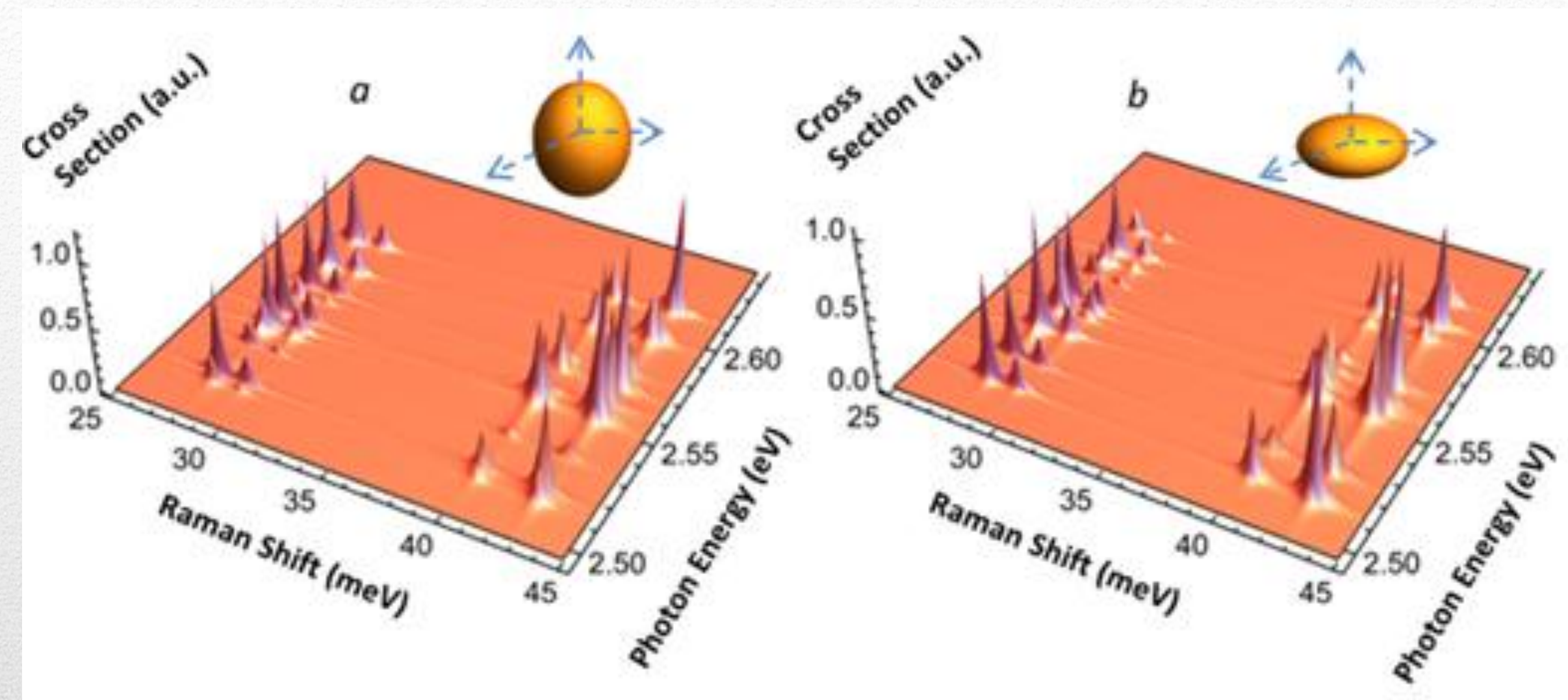
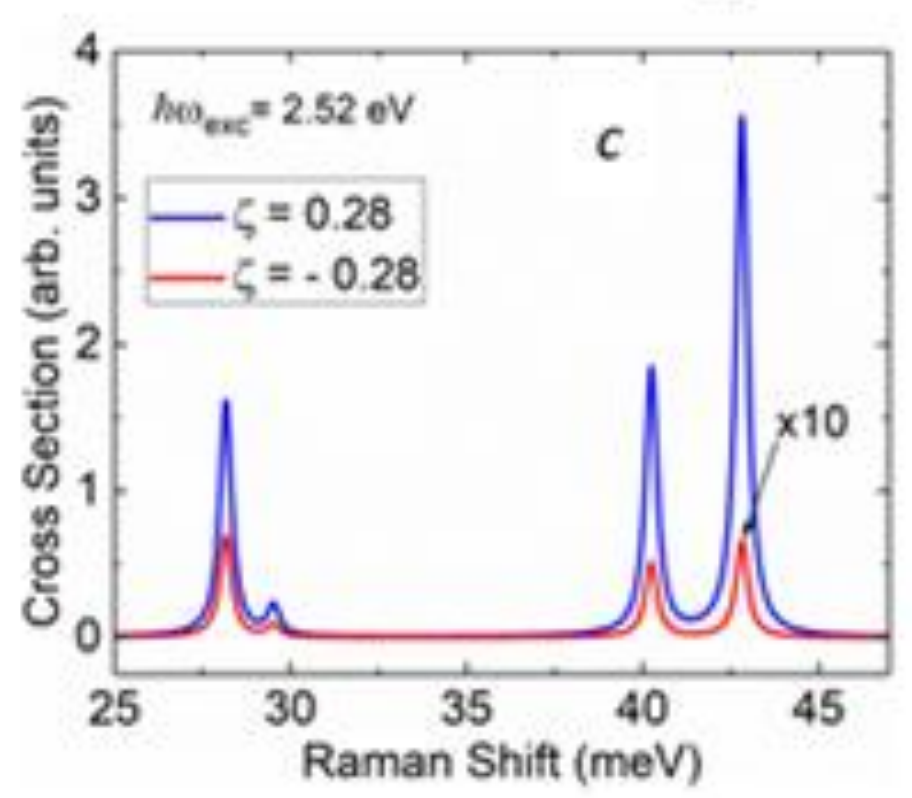


Fig. 6. Computed dependence of the resonance Raman scattering cross-section on the Raman shift and photon energy in the case of a) prolate and b) oblate ellipticity of the core of a core/shell CQD. c) shows Raman shift dependence of the cross-section at excitation energy 2.52eV. The following parameters were used T = 4K, $r_c = 2.3$ nm, $r_s = 2.5$ nm, $|\zeta| = 0.28$.



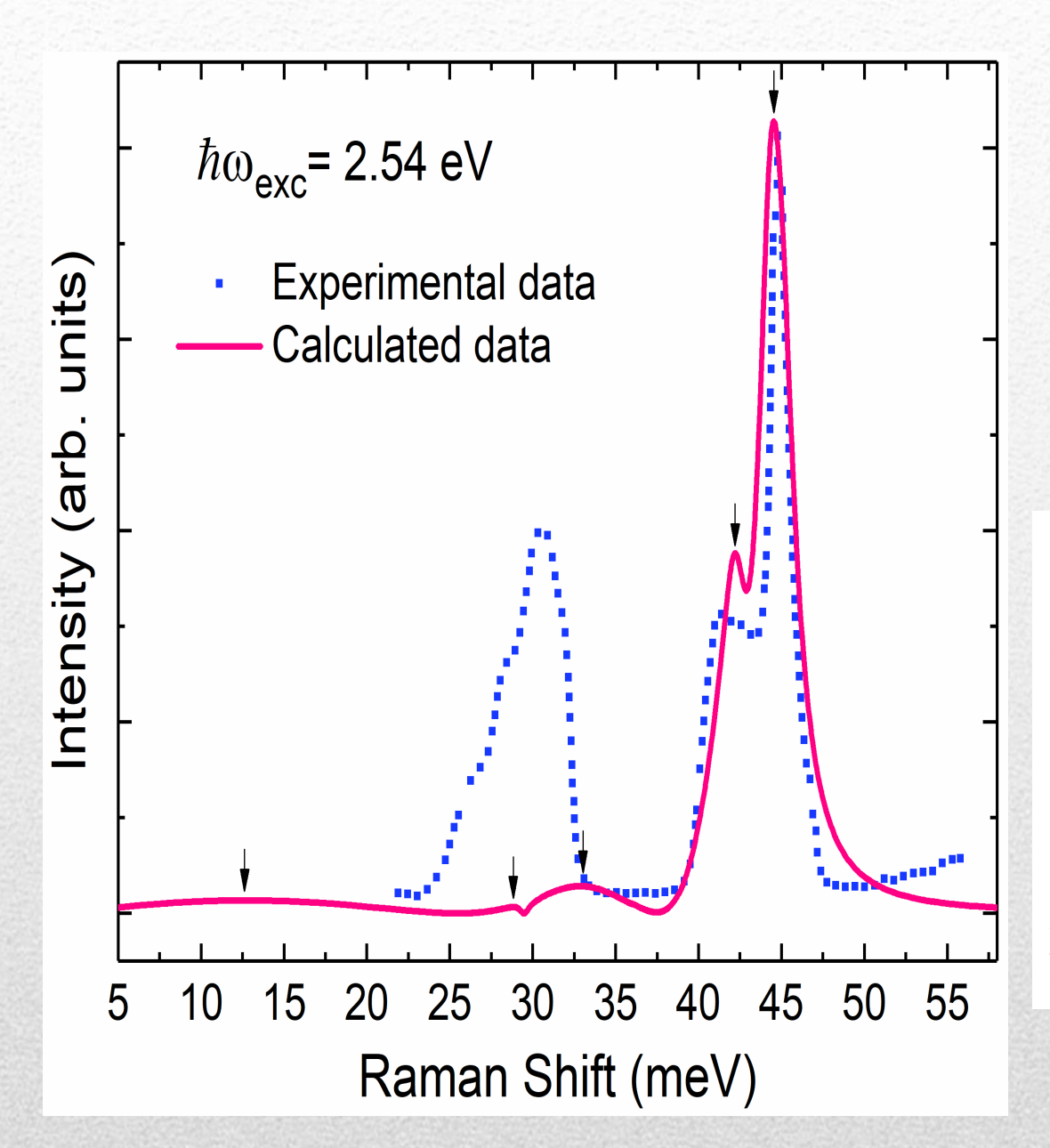


Fig.6. Measured and computed Raman spectra of InP/ZnSe core/shell CQDs with an average core diameter of 2.9 nm at 4K. The incident photon energy is 2.54 eV [20]. The arrows indicate the five Raman frequency shift leading to the expected resonances of the outgoing photons with the five splitted excitonic transitions (Fig. 1).

Conclusion

Our calculated results of the resonant Raman scattering spectra in InP/ZnSe core/shell, a prolate core (zeta equals 0.28), are compared with the experimental data obtained by Brodu et al. The computed results for the Raman intensity as a function of the Raman shift are in excellent agreement with the experimental results both in terms of amplitude and spectral shape in the InP phonon energy range. A frequency shift and a deviation between the experimental and computed amplitude in the phonon range of the ZnSe shell are observed for the interface phonons. It is probably due to the alteration of their frequency by the strain induced by the ZnSe shell, and to the overestimation of the core exciton confinement. These boundary effects have still to be introduced in Raman scattering modeling.

Thanks